



#### RESEARCH PAPER •

Acta Mech. Sin., Vol. 40, 223569 (2024) https://doi.org/10.1007/s10409-024-23569-x

# Chemical short-range-order induced multiscale strengthening in refractory medium entropy alloys

Weizheng Lu<sup>1</sup>, Yang Chen<sup>1\*</sup>, Jia Li<sup>1\*</sup>, Peter K. Liaw<sup>2</sup>, and Qihong Fang<sup>2</sup>

<sup>1</sup> State Key Laboratory of Advanced Design and Manufacturing for Vehicle Body, College of Mechanical and Vehicle Engineering, Hunan University, Changsha 410082, China;

Received December 13, 2023; accepted January 11, 2024; published online May 30, 2024

High/medium entropy alloys (H/MEAs) are generally possible to exhibit chemical short-range order (SRO). However, the complex role of SRO on mechanical properties from nano-scale to meso-scale is still challenging so far. Here, we study the strengthening mechanism and deformation behavior in a model body-centered-cubic HfNbTa MEA by using atomic-scale molecular dynamics, micro-scale dislocation dynamics, and meso-scale crystal plasticity finite element. The SRO inhibits dislocation nucleation at the atomic scale, improving the flow stress. The SRO-induced ultrastrong local stress fluctuation greatly improves the micro-scale dislocation-based strength by the significant dislocation forest strengthening. Moreover, the Ta-rich locally ordered structure leads to an obvious heterogeneous strain and stress partitioning, which forms a strong strain gradient in the adjacent grain interiors and contributes to the strong back-stress-induced strain hardening.

High/medium entropy alloys, Multiscale strengthening, Chemical short-range order

Citation: W. Lu, Y. Chen, J. Li, P. K. Liaw, and Q. Fang, Chemical short-range-order induced multiscale strengthening in refractory medium entropy alloys, Acta Mech. Sin. 40, 223569 (2024), https://doi.org/10.1007/s10409-024-23569-x

#### 1. Introduction

High/medium entropy alloys (H/MEAs) have been growing interest due to the outstanding mechanical properties compared to traditional alloys [1,2]. The truth behind this characteristic is gradually being revealed, mainly attributed to their complex atomic-scale unique microstructures, especially subnanoscale chemical short-range order (SRO) experimentally exhibited [1,2]. The chemical SRO in the CrCoNi MEA is observed using energy-filtered transmission electron microscopy, which causes high stacking-fault energy and hardness [1]. Subsequently, the chemical SRO is explicitly revealed by atomic-resolution imaging and chemical mapping in a face-centered-cubic VCoNi MEA, and its role in plasticity mechanisms and mechanical properties is clarified [2]. Using molecular dynamics (MD) simulation, high yield strength in

\*Corresponding authors. E-mail addresses: yangchen0507@hnu.edu.cn (Yang Chen); lijia123@hnu.edu.cn (Jia Li).

Executive Editor: Xiaoyan Li

CrCoNi MEA is determined by the partial dislocation and nanotwin nucleation, due to the increased slip resistance resulting from SRO [3]. The degree and distribution of chemical SRO would affect the lattice distortion strain fields [4-6], responsible for strain hardening and macroscopic properties [7-10]. However, the influence of chemical SRO on mechanical properties and deformation behavior at different scales is still unclear in the body-centered-cubic (BCC) MEA [11].

#### 2. Methods

#### 2.1 Atomistic simulation

The MD simulations are carried out using a large-scale atomic/molecular massively parallel simulator (LAMMPS) [12]. The MD simulation results are visualized using Ovito code [13]. The embedded atomic method potential describes the interaction of Hf-Nb-Ta atoms [14]. The equilibrate of locally ordered structure is performed by Monte Carlo (MC)/MD simulation [15]. A time step is 1 fs in all MD

<sup>&</sup>lt;sup>2</sup> Department of Materials Science and Engineering, The University of Tennessee, Knoxville TN 37996, USA

simulations. The size of sample is 25 nm  $\times$  25 nm  $\times$  25 nm. The sample is set as periodic boundary conditions for three directions, and equilibrated at zero pressure and room temperature under the isothermal-isobaric (NPT) ensemble. MC steps consist of hybrid MD atomic swap simulations. Based on the Metropolis algorithm in the canonical system. different types of random atoms are reciprocally interchanged. Thus, the as-cast and annealed MEA samples are built. Hence, the constant strain rate of  $1 \times 10^8$  s<sup>-1</sup> is applied along the x-direction. The motion of screw and edge dislocations in the HfNbTa is used to obtain the dislocation drag coefficient using MD simulation. The dislocation mobility of  $1/2 \langle 111 \rangle \{110\}$  edge dislocation and  $1/2 \langle 111 \rangle$ {110} screw dislocation is studied. Energy minimization is performed using periodic boundary conditions along x and y and fixed boundary conditions along z, and then the sample is permitted to relax under canonical (NVT) conditions at room temperature for 100 ps. Under the increasing applied shear load, both screw and edge dislocations experience significant local movement prior to the load.

#### 2.2 Discrete dislocation dynamics simulation

The essence of multiscale modeling is applied to predict the macroscopic mechanical response based on the microscopic physical mechanisms of materials. Due to the need for multiscale models to span huge scales from atomic structure to macroscopic mechanical behavior, it is necessary to model and analyze at some key scales. In this manner, discrete dislocation dynamics (DDD) simulation is used as a bridge between atomic-scale behavior and mesoscale mechanical response. The source code ParaDis is employed to perform all DDD tensile tests in Ref. [16]. We use random field theory to embed the lattice strain field of multi-principal component alloys based on Ref. [17]. The periodic boundary conditions are applied with the simulation box size of 1.8  $\mu$ m  $\times$  1.8  $\mu$ m  $\times$  1.8  $\mu$ m [18]. The initial dislocation density is  $6 \times 10^{12}$  m<sup>-2</sup> with randomly-distributed edge and screw dis-

locations evenly distributed on  $\{110\}$  slip planes, according to the experiment [19,20]. Figure 1(a) shows the initial dislocation configuration of the simulation box. The material parameters for the dislocation behavior of HfNbTa MEA are listed in Table 1 [21]. The loading directions are [001], [101], [102], [112], [111], [212], and [213] orientations [22], and the loading strain rate is  $1 \times 10^4$  s<sup>-1</sup> [23].

A phenomenological dislocation mobility model is applied for DDD simulation [24,25]. The dislocation velocity is expressed as

$$v_s(\tau,T) =$$

$$\begin{cases} \frac{\tau \mathbf{b}}{B_{s}(\tau, T)} \exp\left(-\frac{\Delta G_{kp}(\tau, T)}{2k_{B}T}\right), & \text{if } \Delta G_{kp}(\tau, T) > 0, \\ \frac{\tau \mathbf{b}}{B_{s}(\tau, T)}, & \text{if } \Delta G_{kp}(\tau, T) \leq 0, \end{cases}$$

$$(1)$$

where  $\tau$  is the applied stress, T is the temperature, **b** is the Burgers vector,  $k_{\rm B}$  is the Boltzmann constant.  $\Delta G_{kp}$  is the free enthalpy, the expression is

$$\Delta G_{kp}(\tau, T) = \Delta H_0 \left\{ \left[ 1 - \left( \frac{\tau}{\tau_0} \right)^p \right]^q - \frac{T}{T_0} \right\}, \tag{2}$$

where  $0 \le p \le 1$  and  $1 \le q \le 2$  are fitting parameters,  $\tau_0$  is the Peierls stress,  $T_0$  is a fitting constant. For the case  $\Delta G_{kp}(\tau,T) > 0$ , the active kink-pair mechanism dominates dislocation mobility. Otherwise, the dislocation mobility is controlled by phonon-drag. Therefore, the drag coefficient is written as

$$B_{s}(\tau, T) = \begin{cases} \frac{1}{2} \left[ \frac{\Delta G_{kp}(\tau, T)}{2k_{B}T} \right] \\ \frac{1}{2h_{k}L} B_{k}, & \text{if } \Delta G_{kp}(\tau, T) > 0, \\ B_{0}(T), & \text{if } \Delta G_{kn}(\tau, T) \leq 0, \end{cases}$$
(3)

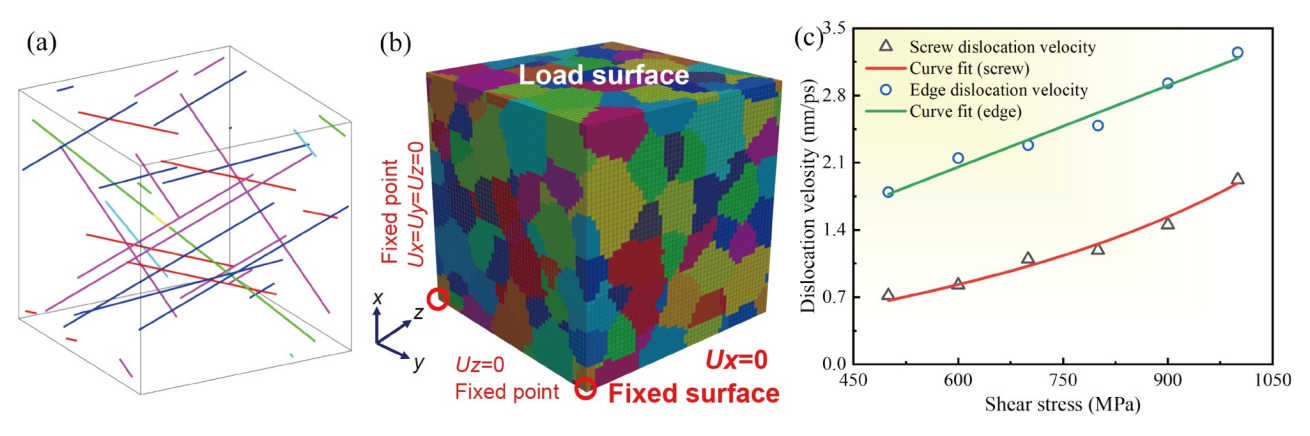


Figure 1 (a) Initial dislocation configuration for DDD simulations; (b) the finite element model of HfNbTa polycrystalline MEA for crystal plastic finite element (CPFE) simulations; (c) the screw and edge dislocation velocity data under different applied shear stress in HfNbTa MEA.

Table 1 Material parameters of HfNbTa MEA for DDD simulations

Symbol	Description	Value	Ref.
а	Lattice constant	0.34 nm	[21]
v	Poisson's ratio	0.3	[21]
$\mu$	Shear modulus	42 GPa	[21]
$h_k$	Kink height	$a\sqrt{2/3}$	[21]
b	Burgers vector	$a\sqrt{3}/2$	[21]

where L is the length of the dislocation line, and  $h_k$  is the kink height.

To obtain the drag coefficient of screw dislocations and edge dislocations, the dislocation velocities under different stresses are calculated using MD simulation. Figure 1(c) shows the edge and screw dislocations velocity data at different shear stresses. Based on Eqs. (1) and (3), the dislocation drag coefficients are obtained through data fitting. The conversion of screw drag coefficient and dislocation velocity is smoothly interpolated by the sigmoidal function, and the squared sum of residual is minimized by the bounded fminsearch function to determine the fitting parameters [24]. The parameters of screw dislocation are  $B_0 = 4.702 \times 10^{-5} \, \text{Pa·s}$ ,  $B_k = 7.815 \times 10^{-5} \, \text{Pa·s}$ , p = 2.791,  $\Delta H_0 = 0.0828$ , and q = 16.182, and the drag coefficient of edge dislocation is  $B = 1.0212 \times 10^{-4} \, \text{Pa·s}$ .

#### 2.3 Crystal plasticity finite element simulation

The PRISMS-Plasticity framework is employed to perform the CPFE simulations in the current work [26]. To calibrate the hardening parameters of polycrystalline representative volume element (RVE), seven single crystal finite element boxes along [001], [101], [102], [112], [111], [212], and [213] have the size of 500  $\mu$ m  $\times$  500  $\mu$ m  $\times$  1,500  $\mu$ m. The displacement boundary condition of x = 0 and two fixed nodes at the bottom are used to prevent movement and rotation of finite element box. The constant strain rate  $1 \times 10^{-3}$  s<sup>-1</sup> is applied along the x-axis direction at room temperature. It is worth noting that the hardening parameters are given by DDD simulations. Figure 1(b) shows the representative volume element model of HfNbTa MEA using CPFE simulation. The polycrystalline model is generated by DREAM. 3D software [27], and set to Voronoi tessellation structure with the average grain size of 20 µm [21]. The simulation box contains 200 grains, which are discretized into 125,000 hexahedral finite elements. The texture of HfNbTa polycrystalline RVE is characterized by randomly oriented grains. The material parameters of CPFE simulations are listed in Table 2 [21,26,28,29].

## 2.4 The methods for bridging simulations at different scales

Two "bridges" are established to connect simulations of

Table 2 Material parameters of HfNbTa MEA in CP constitutive model

Parameter	Description	Value	Ref.
$C_{11}$		191.12	
$C_{12}$	Elastic constant (GPa)	128.88	[21]
$C_{44}$		53.61	
$q_0$	Self-hardening coefficient	1.4	[28,29]
r	Hardening exponent	1.5	[28,29]
m	Sensitivity exponent	0.04	[28,29]
$N_{ m slip}$	Total number of slip systems	12	[26]
$\dot{\gamma}_0$	Reference strain rate (s <sup>-1</sup> )	$10^{-3}$	[26]

different scales. The first bridge coupled nanoscale and microscale simulations: MD simulations calculated the dislocation velocities of screw dislocations and edge dislocations under different stresses, and obtained the dislocation drag coefficient through fitting [21,30], which are then imported into DDD simulations to obtain the interaction behavior of collective dislocations in as-cast HfNbTa MEA during deformation. The strain field caused by lattice distortion and SRO in annealed HfNbTa MEA is simulated by MD/MC simulations. Based on Refs. [31,32], a 3D lattice strain field is constructed using random field theory, and input into DDD simulation to capture the effect of SRO structure on strain hardening in HfNbTa MEA. By establishing single crystal model with seven different crystal orientations ([001], [101], [102], [112], [111], [212], and [213]), the deformation behavior of HfNbTa MEA in both as-cast and annealed states at microscale under uniaxial tension are simulated.

The second bridge coupled microscale and mesoscale simulations: the stress-strain, dislocation density, and shear strain rate of different slip systems obtained from DDD simulations are coupled with the crystal plastic constitutive model, and the hardening parameters of different single crystal orientations required for CPFE simulation are obtained [22]. The physical information with nanoscale SRO and microscale dislocation behavior is transmitted to CPFE simulation. If the hardening parameters with 7 different crystal orientations are treated as random variables, the hardening parameters will follow an approximate normal distribution [22,33]. Therefore, the average values of these hardening parameters can be used in the CPFE model to predict the deformation response of as-cast and annealed HfNbTa MEA [22].

#### 3. Results and discussion

In the present work, the effect of chemical SRO on the mechanical behavior of a BCC HfNbTa MEA at the nanoscale, microscale, and mesoscale is investigated by atomic simulation, DDD simulation, and MD-DDD-CPFE sequential multiscale simulation framework, as shown in

Fig. 2. The strategy for bridging simulations at different scales is included in supplemental materials. At the nanoand micro-scales, based on the atomic simulation, the heterogeneous lattice strain field caused by SRO is transferred to the DDD simulation to study the influence of the chemical concentration fluctuations on the dislocation motion mode. At the meso-scale, the material information with the interaction between dislocations and inhomogeneous strain field is imported into the CPFE simulations. The accuracy and rationality of the simulation results are verified by comparing the predicted stress-strain response with the experimental observations, and the plastic deformation behaviors at the mesoscale are analyzed.

Figure 3(a) exhibits the atomic structures of the as-cast and annealed HfNbTa MEA obtained by different MC/MD cycles [4]. It shows a strong segregation of Ta element and a small amount of segregation of Hf element. These observations are in accordance with the previous experimental results that the Ta-rich cluster and Hf-Zr-rich cluster are easier to form in the HfNbTa-based MEA [34]. The Warren-Cowley parameter  $(\alpha_{ij})$  is commonly used to describe the degree of SRO in MEA, which is given by  $\alpha_{ij}^n = (P_{ij}^n - C_j)/(\delta_{ij} - C_j)$ , where n represents the n-th neighbor shell for i-atom,  $P_{ij}^n$  is the probability of finding an j-type atom on n-th shell,  $C_j$  is the content of j-atom in the system, and  $\delta_{ij}$  is the Kronecker delta. Figure 3(b) shows the Warren-Cowley parameters used to characterize the SRO.

The as-cast sample has no SRO due to the parameters being close to zero (Fig. 3(a) and (b)). The initial random sample has no SRO due to the parameters being close to zero (Fig. 3(b)). The positive values of  $\alpha_{\text{Ta-Ta}}^1$  and  $\alpha_{\text{Hf-Hf}}^1$  for the annealed HfNbTa increase significantly, suggesting that the degree of local Hf and Ta segregation increases (Fig. 3(b)). In addition,  $\alpha^1_{\text{Hf-Nb}}$  is a negative value, which represents a favorable atomic-pair of Hf-Nb. Hence, Fig. 3(a) and (b) reveal the degree and spatial extent of local chemical ordering. The chemical SRO improves not only the yielding strength, but also flow stress (Fig. 3(c)), agreeing with the previous experimental result [2,3]. Figure 3(d) shows the high dislocation density generates as the strain increases. This trend can be ascribed to that the chemical SRO induces a large number of dislocation proliferation (Fig. 3(d)). The corresponding dislocation structure is presented (Fig. 3(e)), and in turn it further validates this result.

To reveal the role of SRO on plastic deformation at the microscale, the as-cast and annealed samples have been simulated by DDD simulation [17]. The strength of the annealed HfNbTa MEA is larger than that of the as-cast sample (Fig. 4(a)), owing to the fact that SRO-induced high local lattice strain hinders the dislocation slip. In the plastic deformation stage, the strain hardening rate of the annealed sample is higher compared to the as-cast sample (Fig. 4(a)). This trend is attributed to the strong toughness caused by the high dislocation density (Fig. 4(b)) [35]. High dislocation

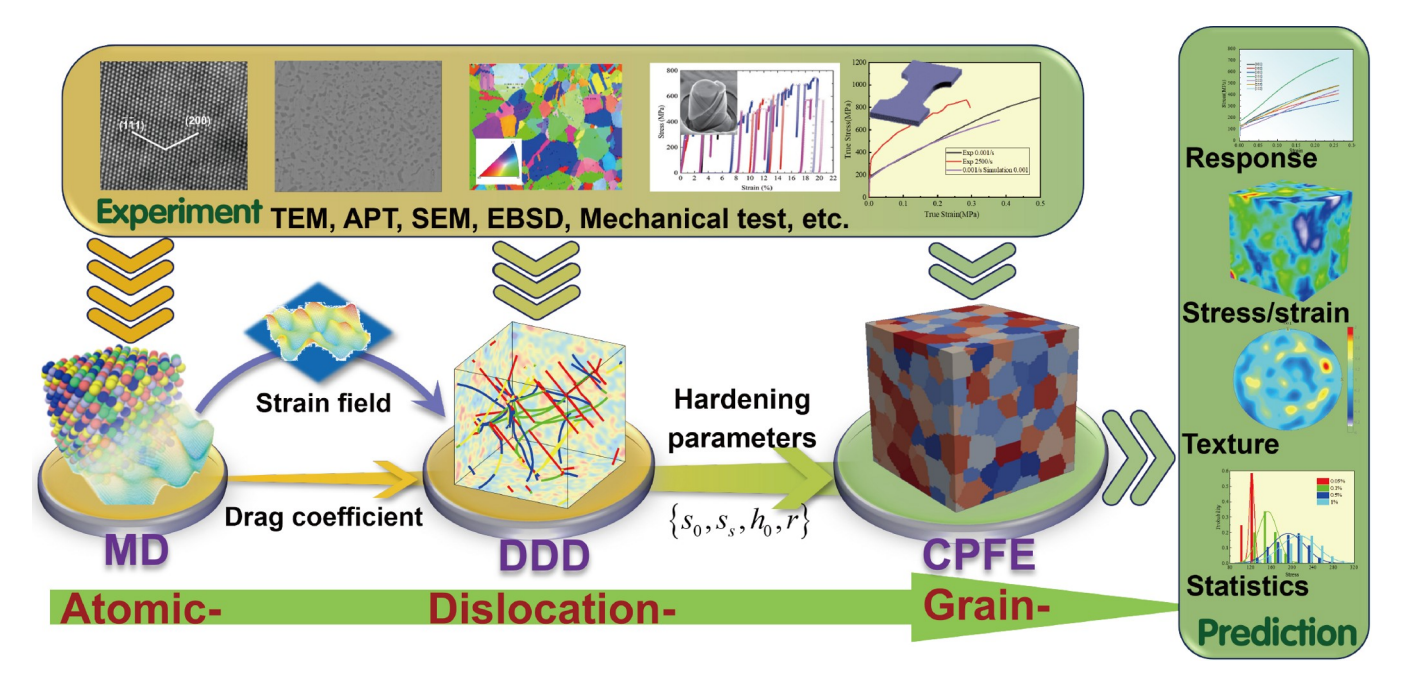
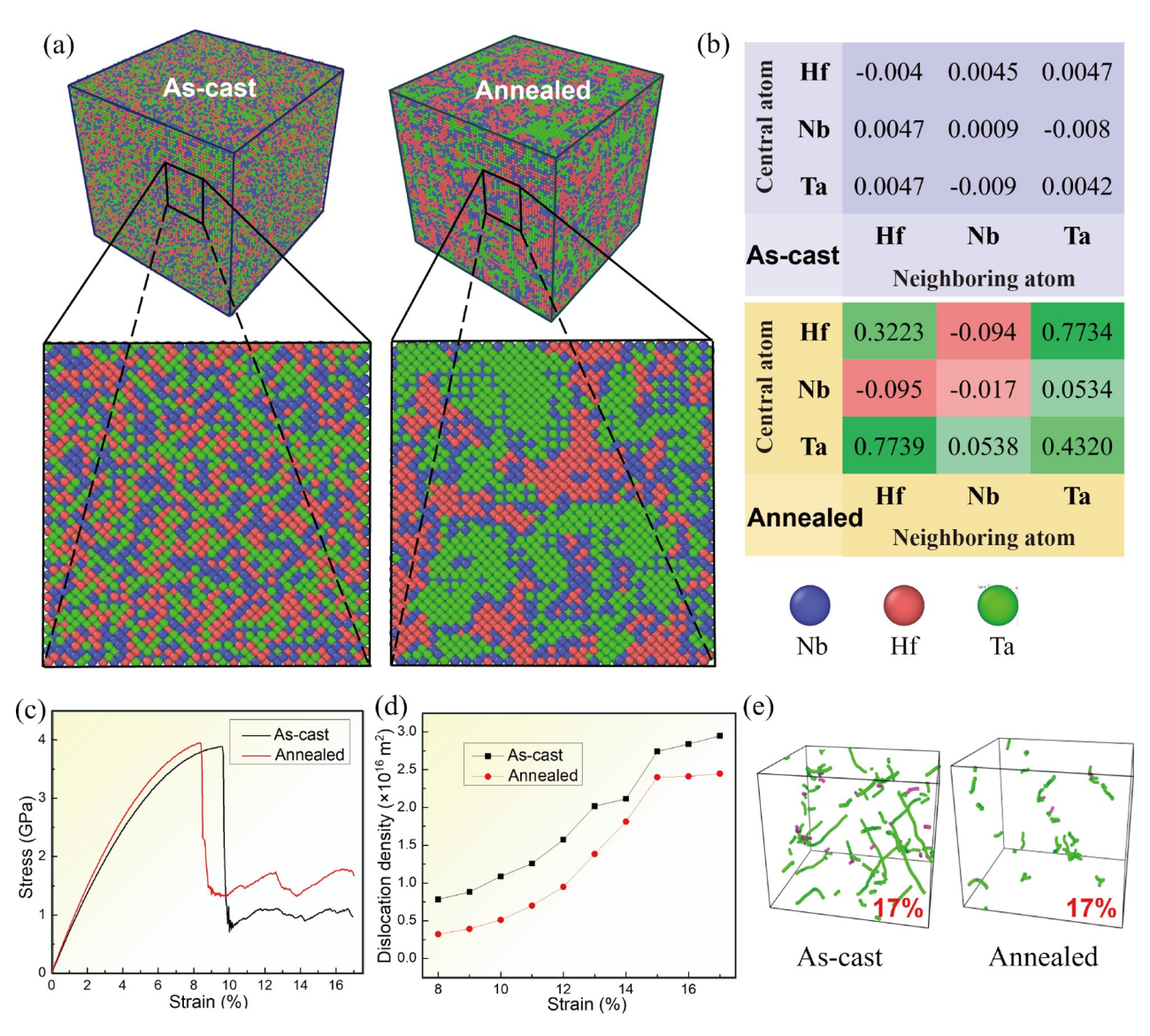


Figure 2 Schematic diagram of MD-DDD-CPFE sequential multiscale modeling strategy, containing atomic simulation, DDD simulation, and CPFE simulation. The multi-scale calculation process includes the five parts: (i) dislocation velocity is simulated through atomic simulation; (ii) the mobility of screw and edge dislocations and the nanoscale heterogeneous strain field are calculated, and then introduced into DDD simulation; (iii) the single crystals of MEA are established to simulate the mechanical behavior through DDD simulation; (iv) by coupling the DDD simulation with crystal plastic model, the hardening parameters of single crystal required for CPFE simulations are calculated. The mechanical response of the single crystal is obtained through CPFE simulation; (v) the stress-strain curve, texture, and stress distribution of the polycrystalline are calculated.



**Figure 3** (a) The atom configurations in the as-cast and annealed HfNbTa samples. (b) The average value of the first nearest neighbor pairwise SRO parameter  $\alpha_{ij}^n$  for the as-cast and annealed samples, where the corresponding samples are described in (a). (c) The stress-strain curves of as-cast and annealed HfNbTa. (d) Dislocation density with the increasing strain. (e) Dislocation structure at a strain of 17%.

density leads to frequent interactions between dislocations, resulting in complex dislocation structures such as jogs and dislocation entanglement, which increases the slip resistance of the dislocation and hinders plastic deformation [36]. The increase of dislocation density caused by cross-slip shows the same trend with the dislocation density, indicating that the dislocation multiplication is mainly due to cross slip (Fig. 4(b)). During the plastic deformation stage, the dislocation density of annealed MEA increases rapidly, while as-cast HfNbTa alloys remain slight net rise. This is due to the frequent occurrence of dislocation cross slip events in MEA (Fig. 4(c) and (d)) [17]. A screw-dislocation slips on the (011) plane, slides on the (101) plane, continues to slide forward, and then slides on the original (011) plane to achieve double cross slip (Fig. 4(e)). Due to the existence of several stress peaks within the range of tens of nanometers in length, hence, the dislocations that cross-slip to an adjacent plane are hindered to continue to cross slip to another adjacent slip plane. As the strain increases, multiple cross slips are activated (Fig. 4(c) and (d)).

Dislocations are hindered at the high lattice stress points induced by the chemical SRO [37], which requires a stronger shear stress to drive dislocation movement. Therefore, when the annealed sample reaches the yield point, it undergoes a high shear stress, which drives the activation of multiple slip systems, thereby increasing the probability of dislocation cross slip to other slip planes [38] (Fig. 4(b) and (c)). This is the intrinsic mechanism behind the growth rate of a high dislocation density in the annealed samples (Fig. 4(b)). The interweaving and entanglement of a high dislocation density in a three-dimensional space generate a large number of immovable dislocations, thereby

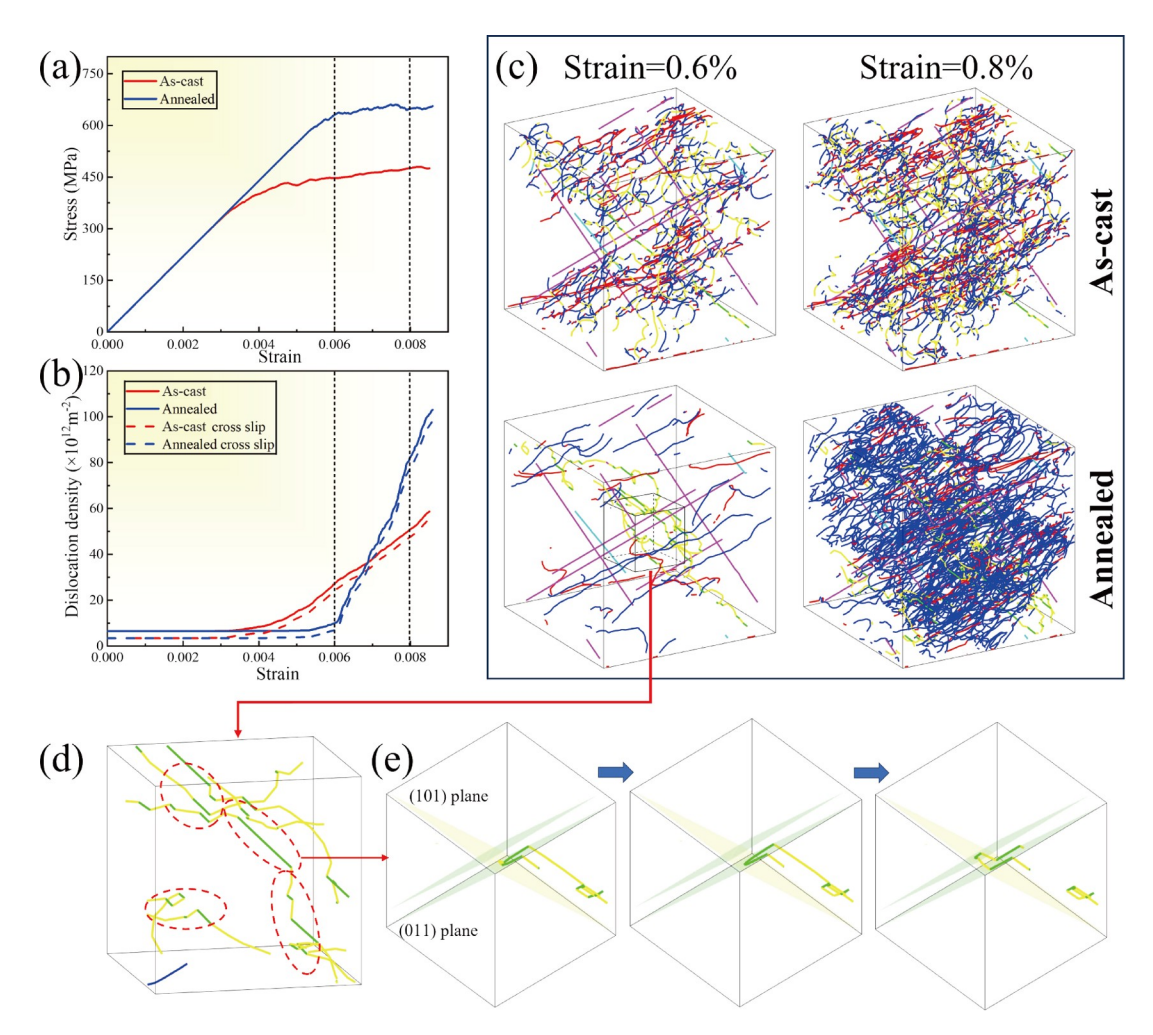


Figure 4 (a) The stress-strain curve; (b) dislocation density and its increase caused by cross slip; (c) dislocation structure along the [001] crystallographic orientation for the as-cast and annealed samples using DDD simulations. Here, the dislocations on the (110) slip plane (cyanine blue), (110) slip plane (pinkish red), (101) slip plane (light-yellow line), (101) slip plane (red line), (011) slip plane (green line), and (011) slip plane (blue line) in (c); (d) the locally enlarged image of the dislocation structure, and the cross slip is marked with red dashed lines; (e) the process of double cross slip.

increasing strain hardening [17,35]. The chemical SRO hinders the dislocation movement in the elastic stage and promotes cross-slip and dislocation proliferation in the plastic stage, which makes it difficult to produce plastic deformation. Thus, the chemical SRO is beneficial for the strength and toughness of MEAs by promoting the rapid proliferation of dislocations.

The mechanical response of the as-cast and annealed HfNbTa MEA at mesoscale is investigated using CPFE simulation [33]. Figure 5(a) shows that the predicted stress-strain curve of the as-cast and annealed HfNbTa polycrystalline in uniaxial tension, compared with the experimental results [21]. The plastic stage of the as-cast HfNbTa is in good agreement with the experimental results (Fig. 5(a)). At the yield point, the experimental result shows the bilinear characteristics, while the CPFE simulation indicates a smooth transition of the gradually accumulated slip strain near the yield point and shows insufficient prediction for the experimental curve (Fig. 5(a)). The maximum error during

the plastic stage is within 5%, occurring at the strain of 9%. It is worth noting that the yield point of the annealed HfNbTa is 132 MPa higher than that of the as-cast sample, and the SRO structure slightly increases the strain hardening rate of the annealed HfNbTa MEA compared to the as-cast sample. The SRO structure hinders the cross-slip and reduces the double-kink nucleation rate of the screw dislocations, resulting in a high strength of MEA [2,39].

The partitioning of the local von Mises stress is one of the important criteria for characterizing the plastic deformation behavior in metallic materials [33]. The von Mises stress statistics for the as-cast and annealed HfNbTa are presented in Fig. 5(b). The as-cast and annealed samples exhibit similar stress distributions, and the annealed HfNbTa MEA exhibits the higher von Mises stress at the same strain level due to the SRO structure (Fig. 5(b)). The Mises stress distribution of as-cast HfNbTa MEA is between 540 and 1,550 MPa, with an average value of 1,036 MPa; the Mises stress distribution of annealed HfNbTa is between 620 and

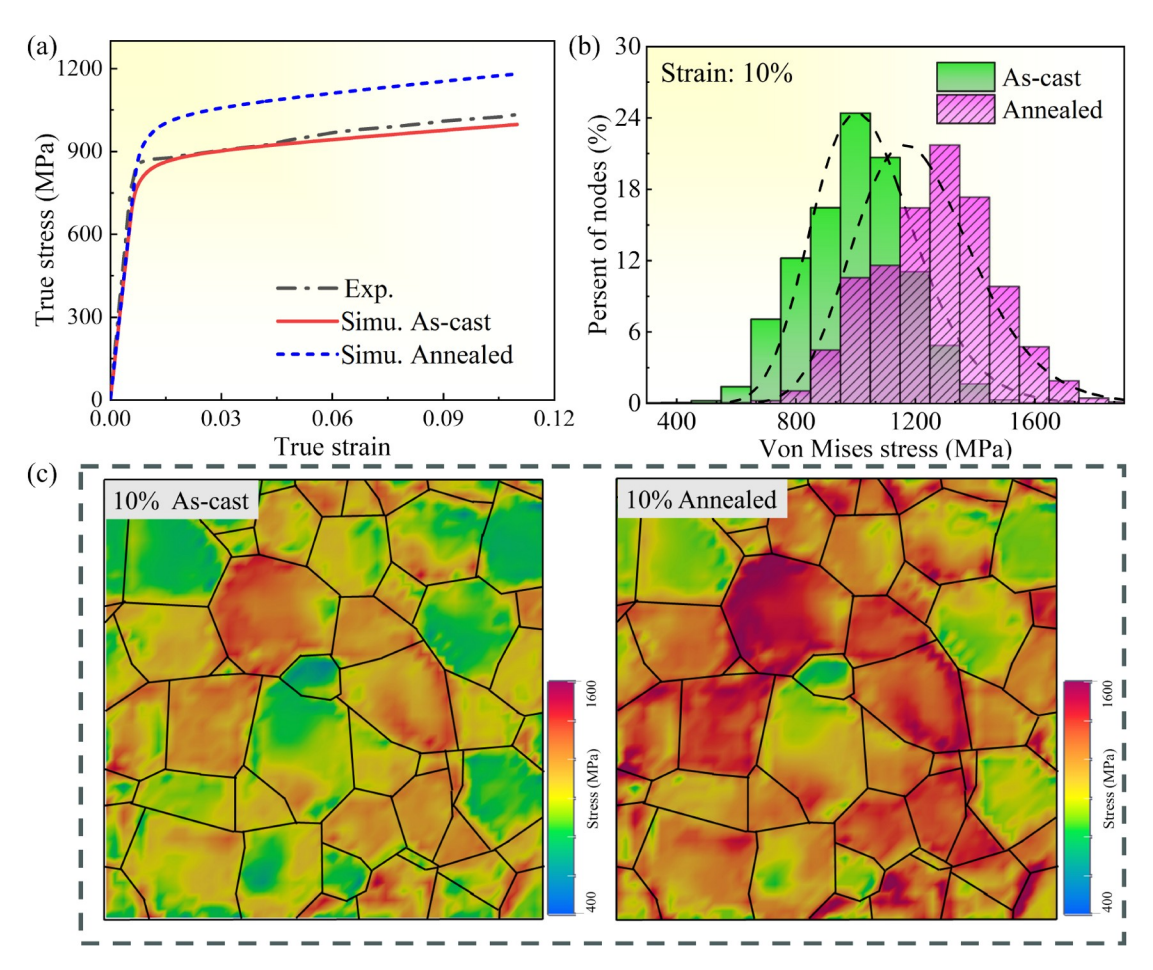


Figure 5 (a) Mechanical response of the as-cast and annealed HfNbTa from the simulated and experimental results; (b) stress statistics (the green area represents as-cast sample, and the red diagonal area represents the annealed sample); (c) stress distribution of the as-cast and annealed HfNbTa at the strain of 10% for plastic stage.

1,800 MPa, with an average value of 1,202 MPa. It indicates that the inhomogeneous degree of the von Mises stress distribution become more serious at the high strain to respond well to the plastic deformation of the high-strength HfNbTa. The von Mises stress distribution at the strain of 10% for the plastic stage is presented in Fig. 5(c). The non-uniformity of the Mises stress distribution in annealed sample become strong, where the areas being close to the high stress gradually increase the stress amplitude. In addition, the heterogeneous stress partitioning surely contributes to the strong back-stress-induced strain hardening in the annealed HfNbTa. Simultaneously, the resultant change of the internal von Mises stress distribution activated by the SRO structure produces the localized and inhomogeneous deformation in some adjacent grains [40].

#### 4. Conclusion

In summary, we propose a crystal plastic method based on the hierarchical multiscale crystal plasticity framework combined with atomic simulation and DDD simulation, to reveal the multiscale strengthening mechanism in the BCC MEA. At the atomic scale, the dislocation nucleation is restrained in the annealed HfNbTa, providing strong flow stress. At the microscale, the local stress fluctuations caused by SRO hinder dislocation slip, resulting in a significant increase in the strength of dislocation junctions for the forest networks. At the mesoscale, the SRO structure leads to an obvious heterogeneous strain and stress partitioning, which forms a strong strain gradient in the adjacent grain interiors, and then contributes to the strong back-stress-induced strain hardening in the annealed HfNbTa. The multiscale crystal plasticity framework is very useful for optimizing and designing the composition heterogeneity of BCC multicomponent alloys to achieve both strength and toughness improvement.

**Conflict of interest** On behalf of all authors, the corresponding author states that there is no conflict of interest.

Author contributions Weizheng Lu: Conceptualization, Methodology, Software, Data curation, Writing – original draft, Visualization, Investiga-

tion, Writing – review & editing. Yang Chen: Methodology, Software, Data curation, Funding acquisition, Writing – original draft, Visualization, Investigation, Writing – review & editing. Jia Li: Methodology, Software, Funding acquisition, Data curation, Writing – original draft, Visualization, Investigation, Writing – review & editing, Supervision. Peter K. Liaw: Writing – review & editing, Project administration, Supervision, Funding acquisition. Qihong Fang: Conceptualization, Methodology, Validation, Writing – review & editing, Supervision, Funding acquisition.

Acknowledgements This work was supported by the National Natural Science Foundation of China (Grant Nos. 12372069, 12302083, and 12172123), China Postdoctoral Science Foundation (Grant Nos. 2023M731061 and BX20230109), the Natural Science Foundation of Hunan Province (Grant No. 2022JJ20001), and Hunan Provincial Innovation Foundation for Postgraduate (Grant No. CX20220378). Peter K. Liaw very much appreciates the support from the National Science Foundation (Grant Nos. DMR-1611180, 1809640, and 2226508).

- R. Zhang, S. Zhao, J. Ding, Y. Chong, T. Jia, C. Ophus, M. Asta, R. O. Ritchie, and A. M. Minor, Short-range order and its impact on the CrCoNi medium-entropy alloy, Nature 581, 283 (2020).
- 2 X. Chen, Q. Wang, Z. Cheng, M. Zhu, H. Zhou, P. Jiang, L. Zhou, Q. Xue, F. Yuan, J. Zhu, X. Wu, and E. Ma, Direct observation of chemical short-range order in a medium-entropy alloy, Nature 592, 712 (2021).
- 3 W. R. Jian, Z. Xie, S. Xu, Y. Su, X. Yao, and I. J. Beyerlein, Effects of lattice distortion and chemical short-range order on the mechanisms of deformation in medium entropy alloy CoCrNi, Acta Mater. 199, 352 (2020).
- 4 Z. Lei, X. Liu, Y. Wu, H. Wang, S. Jiang, S. Wang, X. Hui, Y. Wu, B. Gault, P. Kontis, D. Raabe, L. Gu, Q. Zhang, H. Chen, H. Wang, J. Liu, K. An, Q. Zeng, T. G. Nieh, and Z. Lu, Enhanced strength and ductility in a high-entropy alloy via ordered oxygen complexes, Nature 563, 546 (2018).
- 5 B. Zhang, J. Ding, and E. Ma, Chemical short-range order in body-centered-cubic TiZrHfNb high-entropy alloys, Appl. Phys. Lett. 119, 201908 (2021).
- 6 S. Chen, Z. H. Aitken, S. Pattamatta, Z. Wu, Z. G. Yu, D. J. Srolovitz, P. K. Liaw, and Y. W. Zhang, Simultaneously enhancing the ultimate strength and ductility of high-entropy alloys via short-range ordering, Nat. Commun. 12, 4953 (2021).
- 7 D. Q. Zhao, S. P. Pan, Y. Zhang, P. K. Liaw, and J. W. Qiao, Structure prediction in high-entropy alloys with machine learning, Appl. Phys. Lett. 118, 231904 (2021).
- 8 X. Liu, H. Zhao, H. Ding, D. Y. Lin, and F. Tian, Effect of short-range order on the mechanical behaviors of tensile and shear for NiCoFeCr, Appl. Phys. Lett. 119, 131904 (2021).
- 9 S. Chen, Z. H. Aitken, S. Pattamatta, Z. Wu, Z. G. Yu, D. J. Srolovitz, P. K. Liaw, and Y. W. Zhang, Short-range ordering alters the dislocation nucleation and propagation in refractory high-entropy alloys, Mater. Today 65, 14 (2023).
- 10 S. Xu, W. R. Jian, Y. Su, and I. J. Beyerlein, Line-length-dependent dislocation glide in refractory multi-principal element alloys, Appl. Phys. Lett. 120, 061901 (2022).
- 11 X. Yang, Y. Xi, C. He, H. Chen, X. Zhang, and S. T. Tu, Chemical short-range order strengthening mechanism in CoCrNi mediumentropy alloy under nanoindentation, Scripta Mater. 209, 114364 (2022).
- 12 S. Plimpton, Fast parallel algorithms for short-range molecular dynamics, J. Comput. Phys. 117, 1 (1995).
- 13 A. Stukowski, Visualization and analysis of atomistic simulation data with OVITO—The Open Visualization Tool, Model. Simul. Mater. Sci. Eng. 18, 015012 (2009).
- 14 X. Huang, L. Liu, X. Duan, W. Liao, J. Huang, H. Sun, and C. Yu, Atomistic simulation of chemical short-range order in HfNbTaZr high entropy alloy based on a newly-developed interatomic potential, Mater. Des. 202, 109560 (2021).

- 15 Q. J. Li, H. Sheng, and E. Ma, Strengthening in multi-principal element alloys with local-chemical-order roughened dislocation pathways, Nat. Commun. 10, 3563 (2019).
- 16 V. Bulatov, and W. Cai, Computer Simulations of Dislocations (Oxford University Press, Oxford, 2006).
- 17 J. Li, Y. Chen, Q. He, X. Xu, H. Wang, C. Jiang, B. Liu, Q. Fang, Y. Liu, Y. Yang, P. K. Liaw, and C. T. Liu, Heterogeneous lattice strain strengthening in severely distorted crystalline solids, Proc. Natl. Acad. Sci. U.S.A. 119, e2200607119 (2022).
- 18 A. Arsenlis, M. Rhee, G. Hommes, R. Cook, and J. Marian, A dislocation dynamics study of the transition from homogeneous to heterogeneous deformation in irradiated body-centered cubic iron, Acta Mater. 60, 3748 (2012).
- 19 G. Z. Voyiadjis, and F. H. Abed, Microstructural based models for BCC and FCC metals with temperature and strain rate dependency, Mech. Mater. 37, 355 (2005).
- Y. Cui, G. Po, and N. Ghoniem, Temperature insensitivity of the flow stress in body-centered cubic micropillar crystals, Acta Mater. 108, 128 (2016).
- 21 R. R. Eleti, N. Stepanov, N. Yurchenko, D. Klimenko, and S. Zher-ebtsov, Plastic deformation of solid-solution strengthened Hf-Nb-Ta-Ti-Zr body-centered cubic medium/high-entropy alloys, Scripta Mater. 200, 113927 (2021).
- 22 S. Chandra, M. K. Samal, V. M. Chavan, and S. Raghunathan, Hierarchical multiscale modeling of plasticity in copper: From single crystals to polycrystalline aggregates, Int. J. Plast. 101, 188 (2018).
- 23 H. Fan, Q. Wang, J. A. El-Awady, D. Raabe, and M. Zaiser, Strain rate dependency of dislocation plasticity, Nat. Commun. 12, 1845 (2021)
- 24 G. Po, Y. Cui, D. Rivera, D. Cereceda, T. D. Swinburne, J. Marian, and N. Ghoniem, A phenomenological dislocation mobility law for BCC metals, Acta Mater. 119, 123 (2016).
- 25 Y. Cui, G. Po, P. Srivastava, K. Jiang, V. Gupta, and N. Ghoniem, The role of slow screw dislocations in controlling fast strain avalanche dynamics in body-centered cubic metals, Int. J. Plast. 124, 117 (2020).
- 26 M. Yaghoobi, S. Ganesan, S. Sundar, A. Lakshmanan, S. Rudraraju, J. E. Allison, and V. Sundararaghavan, PRISMS-Plasticity: An opensource crystal plasticity finite element software, Comput. Mater. Sci. 169, 109078 (2019).
- 27 M. A. Groeber, and M. A. Jackson, DREAM.3D: A digital representation environment for the analysis of microstructure in 3D, Integr. Mater. Manuf. Innov. 3, 56 (2014).
- 28 J. H. Kim, M. G. Lee, J. H. Kang, C. S. Oh, and F. Barlat, Crystal plasticity finite element analysis of ferritic stainless steel for sheet formability prediction, Int. J. Plast. 93, 26 (2017).
- 29 Q. Li, H. Zhang, F. Chen, D. Xu, D. Sui, and Z. Cui, Study on the plastic anisotropy of advanced high strength steel sheet: Experiments and microstructure-based crystal plasticity modeling, Int. J. Mech. Sci. 176, 105569 (2020).
- 30 S. Yin, Y. Zuo, A. Abu-Odeh, H. Zheng, X. G. Li, J. Ding, S. P. Ong, M. Asta, and R. O. Ritchie, Atomistic simulations of dislocation mobility in refractory high-entropy alloys and the effect of chemical short-range order, Nat. Commun. 12, 4873 (2021).
- M. Ausloos, and D. H. Berman, A multivariate Weierstrass-Mandelbrot function, Proc. R. Soc. Lond. A 400, 331 (1985).
- 32 H. Zhang, H. Fu, X. He, C. Wang, L. Jiang, L. Q. Chen, and J. Xie, Dramatically enhanced combination of ultimate tensile strength and electric conductivity of alloys via machine learning screening, Acta Mater. 200, 803 (2020).
- 33 Q. Fang, W. Lu, Y. Chen, H. Feng, P. K. Liaw, and J. Li, Hierarchical multiscale crystal plasticity framework for plasticity and strain hardening of multi-principal element alloys, J. Mech. Phys. Solids 169, 105067 (2022).
- 34 S. Maiti, and W. Steurer, Structural-disorder and its effect on mechanical properties in single-phase TaNbHfZr high-entropy alloy, Acta Mater. 106, 87 (2016).

- 35 B. B. He, B. Hu, H. W. Yen, G. J. Cheng, Z. K. Wang, H. W. Luo, and M. X. Huang, High dislocation density-induced large ductility in deformed and partitioned steels, Science 357, 1029 (2017).
- 36 T. W. Zhang, S. G. Ma, D. Zhao, Y. C. Wu, Y. Zhang, Z. H. Wang, and J. W. Qiao, Simultaneous enhancement of strength and ductility in a NiCoCrFe high-entropy alloy upon dynamic tension: Micromechanism and constitutive modeling. Int. J. Plast. 124, 226 (2020).
- 37 Q. Ding, Y. Zhang, X. Chen, X. Fu, D. Chen, S. Chen, L. Gu, F. Wei, H. Bei, Y. Gao, M. Wen, J. Li, Z. Zhang, T. Zhu, R. O. Ritchie, and Q. Yu, Tuning element distribution, structure and properties by composition in high-entropy alloys, Nature 574, 223 (2019).
- 38 F. Wang, G. H. Balbus, S. Xu, Y. Su, J. Shin, P. F. Rottmann, K. E. Knipling, J. C. Stinville, L. H. Mills, O. N. Senkov, I. J. Beyerlein, T. M. Pollock, and D. S. Gianola, Multiplicity of dislocation pathways in a refractory multiprincipal element alloy, Science 370, 95 (2020).
- 39 S. Yin, J. Ding, M. Asta, and R. O. Ritchie, Ab initio modeling of the energy landscape for screw dislocations in body-centered cubic highentropy alloys, Npj Comput. Mater. 6, 110 (2020).
- 40 S. Tsianikas, Y. Chen, A. Slattery, J. Peters, and Z. Xie, Adaptive attenuation of hierarchical composition fluctuations augments the plastic strain of a high entropy steel, Mater. Sci. Eng.-A 857, 144037 (2022).

### 难熔中熵合金化学短程有序强化的多尺度模拟研究

鲁卫征、陈阳、李甲、Peter K. Liaw、方棋洪

摘要 中熵合金中广泛存在的化学短程有序对材料强韧性的影响研究是一个典型的跨尺度问题,构建从纳米尺度结构细节到细观尺度力学性能的跨尺度关联方法是阐明化学短程有序强韧化机理的关键。我们发展了一套结合纳米尺度分子动力学、微米尺度离散位错动力学和介观尺度晶体塑性有限元的分层多尺度模型框架。基于该方法,我们以体心立方HfNbTa体系为例,系统研究了化学短程有序对典型难熔中熵合金变形和强化行为的影响机理。纳米尺度上,化学短程有序结构抑制了位错形核,从而提高了合金的流动应力;细观尺度上,化学短程有序引起的超强局部应力波动诱发了额外的林位错强化,显著提高了位错强化的贡献。此外,通过诱导富Ta局部有序结构的形成,合金中的原子级非均匀应变和应力能够进一步增强,从而在相邻晶粒内部形成强应变梯度,提升背应力诱导的应变硬化。